An Efficient Oscillator Design Based on OTA Nonlinearity

Kofi M. Odame, Paul Hasler
School of Electrical and Computer Engineering
Georgia Institute of Technology, Atlanta, Georgia 30332–0250
odame@ece.gatech.edu

***Abstract*— An analog sinusoidal oscillator usually involves some form of amplitude-limiting mechanism. We examine OTA nonlinearity as a choice for amplitude limiting, and introduce a general method for its use in OTA-C oscillators. We illustrate our discussion with an example design that we fabricated and tested. Our results show that OTA nonlinearity yields low-distortion oscillators at practically no power- or area cost.**

I. Oscillator Amplitude-Limiting

We present a general method for using OTA nonlinearity as an amplitude limiter in OTA-C sinusoidal oscillators. Several researchers have recognized the possibility of exploiting OTA nonlinearity as such [1]–[3]. However, few have used it successfully to achieve reasonably-undistorted sinusoids [4]. We show in this paper that OTA nonlinearity is a practical and generally-applicable amplitude-limiting scheme in oscillator design. Our method avoids using a piece-wise linear model of the OTA, which would result in uncontrollable, distorted oscillation [3]. Further, our use of inherent circuit nonlinearity eliminates the need for such external-limiting mechanisms as automatic gain control (AGC), thus achieving an area- and power-efficient design. Small, low-power circuitry is essential in biological signal processing, and we illustrate our design method with results from a compact, micropower oscillator.

In order to maintain low distortion levels, most of the OTAs in the oscillator circuit must be linear. A single nonlinear OTA is however all that is needed to ensure stable oscillations. We will address the specific details of how to bias the nonlinear OTA, and how to place it in an otherwise linear OTA-C circuit in order to achieve low-distortion oscillations.

We have organized this paper as follows. Section II introduces the OTA and its transfer function equations. Section III describes the synthesis method and oscillator architecture. In Section IV, we validate our technique with a simple OTA-C second-order section, which we fabricated in a 0.5μm CMOS process. Finally, we make some comparisons between our scheme and other amplitude-limiting techniques for OTA-C oscillator design.

II. Linear and Nonlinear OTAs

A differential pair is at the heart of the typical OTA. The OTA's differential voltage input, $V_{\rm in} = V_+ - V_-$, is applied to the differential pair. A current subtraction network generates the difference of the differential pair's drain currents, $I_{\rm out} = I_+ - I_-$. The OTA thus provides a *transconductance* function from $V_{\rm in}$ to $I_{\rm out}$.

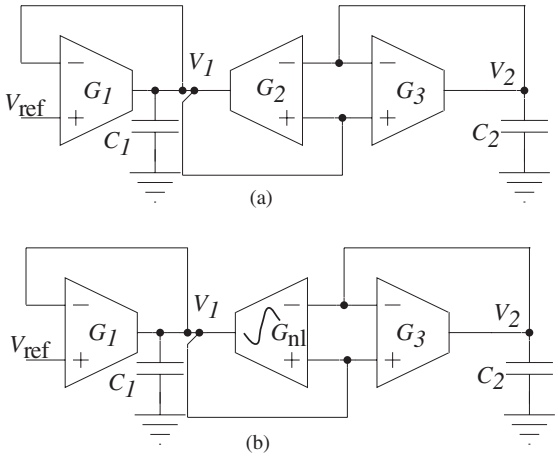

Fig. 1. SOS conversion to an oscillator. (a) Original circuit. All of the OTAs are linear, and the circuit is small-signal stable. (b) OTA-C oscillator circuit. Replacing G_2 with the nonlinear OTA, $G_{\rm nl}$, converts the circuit into a van der Pol's oscillator.

Depending on the differential pair's region of operation[1], the OTA's output current is

$$I_{\rm out} = \begin{cases} I_{\rm bias} \tanh\left(\frac{\kappa V_{\rm in}}{2U_{\rm T}}\right) & \text{subthreshold,} \\ V_{\rm in}\sqrt{\kappa\beta I_{\rm bias} - (\kappa\beta V_{\rm in}/2)^2} & \text{above threshold,} \end{cases} \quad (1)$$

where κ is the body-effect coefficient and $U_{\rm T}$ is the thermal voltage. $I_{\rm bias}$ is a tunable bias current. Also, β is a physical constant that is related to the differential pair's geometry and to doping concentrations.

The subthreshold transconductance function has the following Taylor-series expansion

$$I_{\rm out} = \frac{\kappa I_{\rm bias}}{2U_{\rm T}}\left(V_{\rm in} - \frac{\kappa^2 V_{\rm in}^3}{12U_{\rm T}^2}\right) + {\rm O}(V_{\rm in}^4). \quad (2)$$

For above threshold, it is

$$I_{\rm out} = \sqrt{\kappa\beta I_{\rm bias}}\left(V_{\rm in} - \frac{\kappa\beta V_{\rm in}^3}{8I_{\rm bias}}\right) + {\rm O}(V_{\rm in}^4). \quad (3)$$

[1]We restrict our discussion to CMOS design. However, the results in this paper are directly applicable to BJT and BiCMOS technologies.

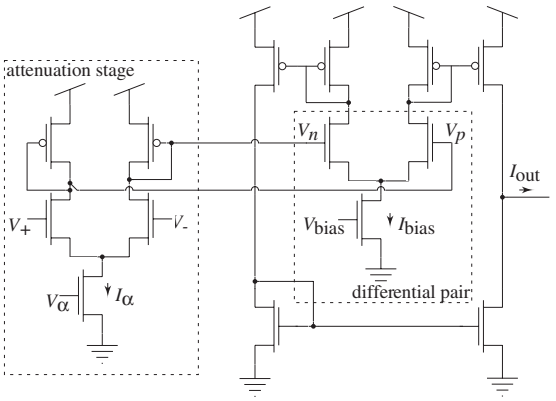

Fig. 2. The variable linear range OTA. Voltage attenuation between V_+, V_- and V_p, V_n results in a linear transfer function. The amount of linearity is controlled by the bias current, I_α.

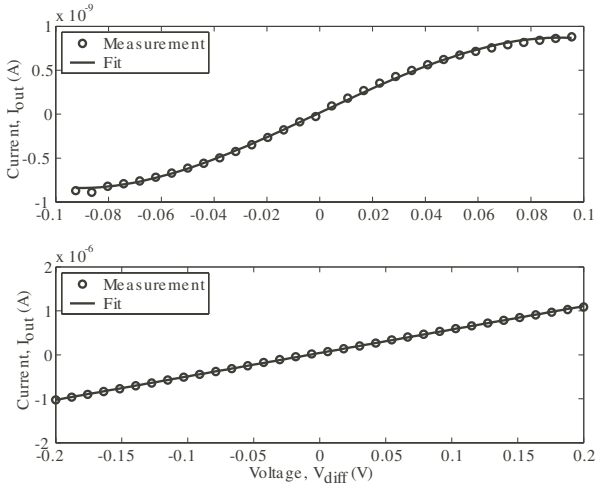

Fig. 3. OTA transfer curves. The upper panel depicts a weakly nonlinear transfer curve, which is approximated by a linear- and a cubic-termed polynomial. In the lower panel, the nonlinear terms are suppressed enough for a straight line to be an accurate approximation.

So, regardless of its region of operation, a differential-pair OTA's transfer function has got a positive linear term and a negative cubic term. The coefficient of the linear term is called the small-signal transconductance gain, and is denoted as $G_{\rm m}$. We obtain a linear OTA via *linearization* [5], which would make the cubic term (and all other higher-order terms) of the transfer function negligible . Similarly, we may *weakly nonlinearize* an OTA, whereby the cubic term becomes significant to the linear term, while all of the other higher-order terms remain negligible. We refer to such an element as a nonlinear OTA.

III. Oscillator Architecture

The most common design for a sinusoidal oscillator consists of a second-order section (SOS) and some amplitude-limiting mechanism [1]–[4]. In our case, the amplitude-limiting mechanism is a cubic nonlinearity. Borrowing from nonlinear dynamical systems theory, we may frame our design problem as a circuit implementation of the van der Pol equation [6]. Van der Pol's equation is the quintessential second-order oscillator that operates via cubic nonlinearity, and is written as

$$\ddot{y} - \epsilon(1 - y^2)\dot{y} + y = 0, \quad \epsilon > 0, \tag{4}$$

where y represents the oscillator's output voltage, and ϵ is a measure of the nonlinear OTA's transconductance gain relative to that of the other OTAs.

The van der Pol equation can be synthesized with *any* small-signal stable, linear OTA-C SOS, as long as it is properly coupled with a nonlinear OTA. The SOS consists of linear OTAs and two grounded capacitors, each connected to one of the two dominant-pole nodes of the circuit. The specific topology of the SOS could depend on considerations like low noise and low distortion, as discussed in [7].

Given a stable SOS, we couple in a nonlinear OTA as follows. The nonlinear OTA's output current should be sourced onto one of the dominant-pole nodes of the SOS. The voltage input of the nonlinear OTA should be directly proportional to the current that is sunk by the capacitor on the SOS's other node. Once in this configuration, there is a threshold transconductance gain of the nonlinear OTA, past which it will destroy the stability of the SOS. This onset of instability is the start-up condition for the oscillator, and thus completes the van der Pol synthesis.

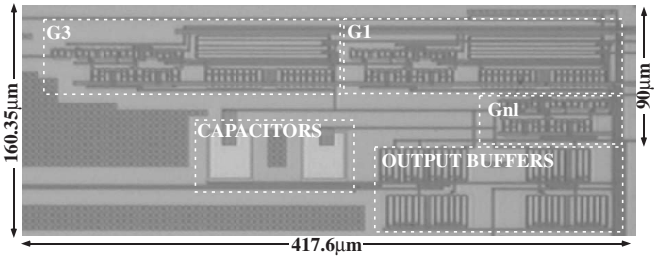

Fig. 4. Oscillator die micrograph. The labeled portions correspond to the circuit components in Fig. 1(b). Total area, including output buffers, is $160.35\mu\text{m} \times 417.60\mu\text{m}$.

IV. Prototype Circuit

We applied our oscillator design methodology to the OTA-C circuit depicted in Fig. 1(a), which is a classical low power SOS for biological signal processing [8]. Note, we could have synthesized the oscillator out of a circuit optimized for noise and distortion performance, rather than for power efficiency. Our oscillator circuit was fabricated in a 0.5μm CMOS process available from MOSIS.

A. Identification of the Nonlinear OTA

The OTA-C circuit of Fig. 1(a) is small-signal stable, and hence convertible into the van der Pol oscillator. For the conversion, we chose to place a nonlinear OTA into the circuit such that its output current was sourced onto node V_1. Also, the input to the nonlinear OTA had to be proportional to the

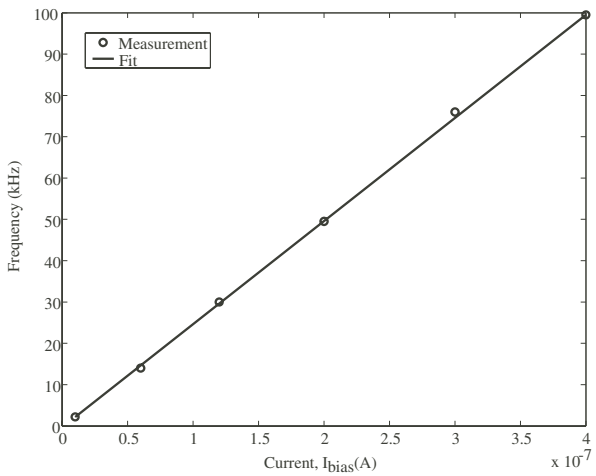

Fig. 5. Linear frequency control with current $I_{\rm bias}$, at 100mV$_{\rm pp}$ oscillation amplitude. The transconductance gain of every OTA in Fig. 1(b) is defined by $I_{\rm bias}$. Increasing the current increases each transconductance gain proportionally, causing a linear increase in the oscillation frequency.

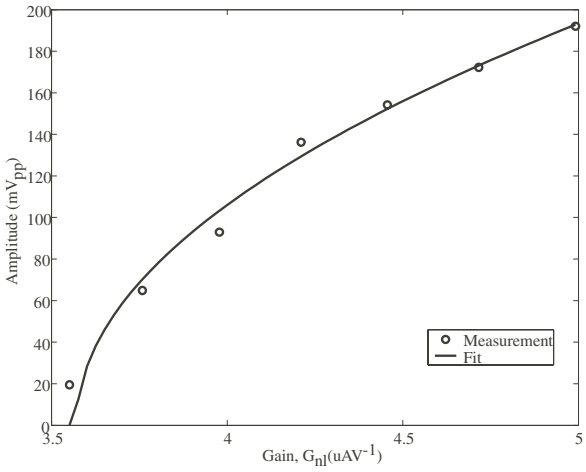

Fig. 6. Amplitude control with transconductance $G_{\rm nl}$, at 100kHz oscillation frequency. The transconductance $G_{\rm nl}$ is directly proportional to ϵ. From basic nonlinear analysis the amplitude of oscillation is proportional to $\sqrt{\epsilon}$, for small enough ϵ.

current being sunk by capacitor C_2. Applying KCL to node V_2, we calculated that the nonlinear OTA's input must be a multiple of $V_1 - V_2$. Notice that the inputs and output of the transconductance element G_2 exactly fulfil the placement requirements for our nonlinear OTA. So, our synthesis procedure was completed by simply replacing the linear OTA G_2 with a nonlinear one, $G_{\rm nl}$, which is depicted in Fig. 1(b).

B. Circuit Implementation

The two linear OTAs, G_1 and G_3, were each implemented as the variable linear range OTA of Fig. 2 [9]. The bias current of the attenuation stage controls the linear range of the OTA. The nonlinear OTA, $G_{\rm nl}$, was implemented as a simple nine-transistor OTA. The data in Fig. 3 shows the linear and nonlinear characteristics of the respective OTAs.

The complete oscillator circuit had a bounding box of $160.35\mu{\rm m} \times 417.60\mu{\rm m}$, as shown in the die photo of Fig. 4. The nodes V_1 and V_2 were accessible via on-chip buffers. We controlled the bias currents through the bias transistors' gate voltages. The OTAs ran on a single-ended supply of 3.3V and had a bandwidth of a few hundred kHz.

C. Experimental Results

Contrary to other results, such as in [3], our systematic exploitation of OTA nonlinearity does produce a well-analyzed and understood oscillator. From nondimensionalization analysis of the van der Pol oscillator [10], we expect the following expression for frequency of oscillation

$$f_{\rm osc} = G/C_1, \tag{5}$$

where G is the OTAs' mean transconductance gain. We set $G_1 = G_3 = G$ for simplicity. Then, assuming subthreshold operation, we may define

$$G_{1,3} = \frac{\kappa I_{\rm bias}}{2U_{\rm T}}, \quad G_{\rm nl} = \frac{\kappa a I_{\rm bias}}{2U_{\rm T}}. \tag{6}$$

The frequency of oscillation should then be linearly dependent on $I_{\rm bias}$. In Fig. 5, our experimental results show a linear tuning range of 2.2kHz to 100kHz. The power consumption varies over this tuning range from 0.19μW to 6.27μW. If we opt for above-threshold operation, we can push the frequency of oscillation into the low 200kHz range. We emphasize that the OTAs were designed for kHz operation. As evinced in [4], OTA nonlinearity is *not* a limitation on the maximum oscillation frequency.

The perturbation method of first-order averaging [11] finds the following relationship between ϵ and oscillation amplitude

$$v_{\rm amp} \propto \frac{1}{\sqrt{1 + 2/\epsilon}}, \tag{7}$$

which is a square-law, for small enough ϵ. For our prototype oscillator, the ϵ term is defined as $\epsilon = G_{\rm nl}/G - 2$. Keeping G constant, we expect a square-law relationship between $G_{\rm nl}$ and the oscillation amplitude. The results in Fig. 6 confirm this relationship.

High-order perturbation analysis of the van der Pol equation predicts that the total harmonic distortion (THD) is due strictly to odd-order harmonics, and is given by

$$\begin{aligned} {\rm THD}\ \% &= \frac{\epsilon}{8}\sqrt{\frac{1 + 349\epsilon/576}{1 + \epsilon^2/64 + \epsilon^4/256}} \cdot 100 \\ &\approx 25\epsilon/2. \end{aligned} \tag{8}$$

Fig. 7(b) shows the oscillator's output power spectrum for a peak-to-peak amplitude of 90mV, at a frequency of 146kHz. The THD at this output level is 0.47%. The prominent second-order harmonic is due to differential-pair input offset, which has been magnified by the attenuation stage of Fig. 2. To eliminate even-order harmonics, the OTAs must be designed using such offset-removal techniques as those described in [12].

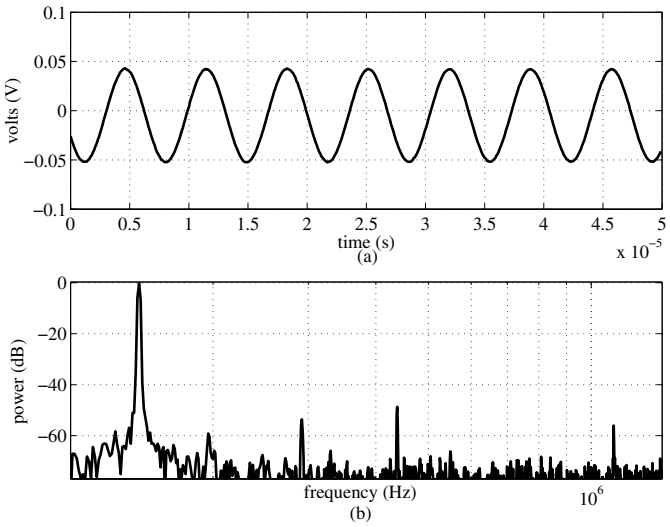

Fig. 7. Oscillator output for 90mV_{pp} at 146kHz. (a) Timeseries. (b) Power spectrum. The even-order harmonics are due to input offset in the linear OTAs. THD calculated up to the 10^{th} harmonic is 0.47%. Phase noise is -66dBc/Hz at a 10kHz offset.

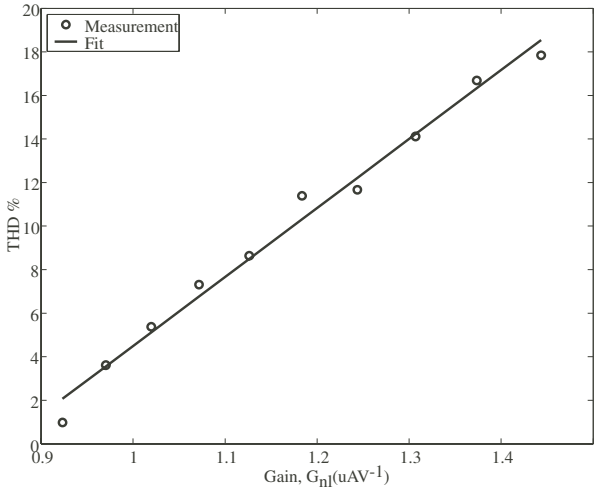

Fig. 8. Total harmonic distortion (THD) exhibits a linear dependence on transconductance gain G_{nl}, as predicted by perturbation theory. These THD measurements are for an oscillation frequency of 20kHz, and include harmonics up to the 10^{th}.

Our experimental results in Fig. 8 do show a fairly linear increase in THD with respect to G_{nl} and hence ϵ, as expected from perturbation theory. Observe that both amplitude and THD increase with G_{nl}. To avoid distortion in large-amplitude oscillations, we can stretch out the nonlinear transfer function. For instance, making the cubic law hold for a 500mV range, instead of for the 200mV range depicted in Fig. 3, will allow for low-distortion, large amplitude oscillations.

V. Discussion and Conclusion

We have presented a general scheme for exploiting OTA nonlinearity for amplitude-limiting in OTA-C sinusoidal oscillators. We illustrated the practicability of our scheme with a prototype oscillator that was fabricated in a 0.5μm technology. Table I compares our method with the two more-commonly used amplitude-limiting techniques. These are AGC and a piecewise linear limiter (PWL). An AGC requires such added circuitry as a peak detector and bias control, but it results in low THD oscillators. A PWL can have a fairly compact design, but it often causes slightly worse THD than does AGC. With OTA nonlinearity, the question of extra circuitry does not apply, because the amplitude-limiting mechanism is integrated into the SOS's dynamics. The designer has but to identify the proper placement of the nonlinear OTA in a SOS, for it to be an oscillator. The THD performance of such an oscillator is at least as good as that of a PWL.

TABLE I

Comparison of Amplitude-Limiting Schemes in Oscillators

	AGC	PWL	OTA Nonlinearity
Extra Area	high	low	none
Extra Power	high	low	none
Complexity	high	low	low
THD	low	low-moderate	low

References

[1] A. Buonomo, C. Di Bello, and A. Lo Shiavo, "On the analysis and design of second-order harmonic oscillators," in *Proc. ISCAS'00*, May 2000, vol. 1, pp. 623–626.

[2] B. Linares-Barranco, A. Rodriguez-Vazquez, E. Sanchez-Sinencio, and J.L. Huertas, "Cmos ota-c high-frequency sinusoidal oscillators," *IEEE Journal of solid-state circuits*, vol. 26, no. 2, pp. 16–165, 1991.

[3] A. Rodriguez-Vazquez, B. Linares-Barranco, J.L. Huertas, and E. Sanchez-Sinencio, "On the design of voltage-controlled sinusoidal oscillators using ota's," *IEEE Trans. Circuits Syst.*, vol. 37, no. 2, pp. 198–211, 1990.

[4] J. Galan, R.G. Carvajal, A. Torralba, F. Munoz, and J. Ramirez-Angulo, "A low-power low-voltage ota-c sinusoidal oscillator with a large tuning range," *TCASI: Fundamental Theory and Applications*, vol. 52, no. 2, pp. 283–291, 2005.

[5] B. Razavi, *Design of Analog CMOS Integrated Circuits*, McGraw Hill, New York NY, 2001.

[6] B. Van der Pol, "On relaxation oscillations," *Philos. Mag.*, vol. 27, pp. 978–992, 1926.

[7] S. Koziel, R. Schaumann, and H. Xiao, "Analysis and optimization of noise in continuous-time ota-c filters," *TCASI: Fundamental Theory and Applications*, vol. 52, no. 6, pp. 1086–1094, 2005.

[8] R.F. Lyon and C. Mead, "An analog electronic cochlea," *IEEE Trans. on Acoustics, Speech and Signal Proc.*, vol. 36, no. 7, pp. 1119–1134, 1988.

[9] S.P. DeWeerth, G.N. Patel, and M.F. Simoni, "Variable linear-range subthreshold ota," *Electronics Letters*, vol. 33, no. 15, pp. 1309–1311, 1997.

[10] S. H. Strogatz, *Nonlinear Dynamics and Chaos*, Westview, Cambridge, MA, 1994.

[11] R. Rand, *Lecture Notes on Nonlinear Vibrations*, The Internet-First University Press, Ithaca, NY, 2003.

[12] V. Srinivasan, G. J. Serrano, J. Gray, and P. Hasler, "A precision cmos amplifier using floating-gates for offset cancellation," in *Proc. CICC'05*, Sept. 2005, pp. 734–737.